Scheme II

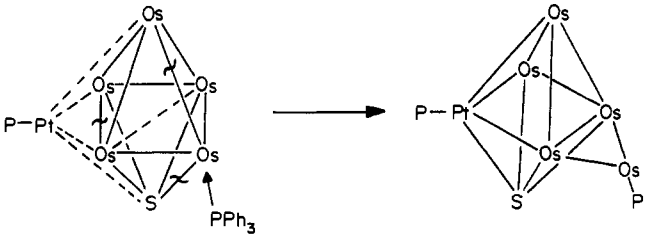

to this osmium group also occurs. These clusters decarbonylate by reincorporating the osmium group into the cluster and shifting the platinum atom onto the triosmium face. A similar process could lead to the formation of **4**. Unfortunately, we have not observed the expected precursor (i.e. the carbonyl analogue of **6**, $PtOs_5(CO)_{16}(PPh_3)(\mu_4\text{-}S)$). However, it was observed that the yield of **4** was increased to 13% when the reaction of **1** and $Pt(PPh_3)_2C_2H_4$ was performed under a atmosphere of carbon monoxide. Compound **6** decomposes not by condensation, but by loss of metal-containing units. By loss of the edge-bridging $Os(CO)_3PPh_3$ group, compound **2** is formed. However, reincorporation of this osmium bridge is a competing process and this leads to formation of **3** via loss of a platinum containing moiety.

Acknowledgment. This research was supported by the National Science Foundation under Grant No. CHE-8416460. We wish to thank Johnson-Matthey for a loan of osmium tetroxide.

Registry No. **1**, 86437-19-6; **2**, 101566-39-6; **3**, 99595-19-4; **4**, 101629-48-5; **6**, 101566-41-0; **7**, 101566-42-1; $Os_4(CO)_{11}(NMe_3)(\mu_3\text{-}S)$, 101566-43-2; $Pt(PPh_3)_2(C_2H_4)$, 12120-15-9; Os, 7440-04-2; Pt, 7440-06-4.

Supplementary Material Available: Tables of anisotropic thermal parameters for all three structures and hydrogen atom coordinates for compounds **2** and **4** (5 pages). Ordering information is given on any current masthead page. According to policy instituted Jan 1, 1986, the tables of calculated and observed structure factors (116 pages) are being retained in the editorial office for a period of 1 year following the appearance of this work in print. Inquiries for copies of these materials should be directed to the Editor.

Contribution from the Department of Chemistry,
Simon Fraser University, Burnaby, British Columbia, Canada V5A 1S6

Synthesis, Structures, and Nonrigidity of Heterotrimetallic Alkyne Clusters of the Type $CpNiCoM(CO)_6(C_2RR')$ (M = Fe, Ru, Os)

Frederick W. B. Einstein, Kenneth G. Tyers, Alan S. Tracey, and Derek Sutton*

Received July 23, 1985

A series of heterotrimetallic alkyne clusters of the type $CpNiCoM(CO)_6(C_2RR')$ (where M = Fe, Ru, Os) has been synthesized and structurally investigated. In all cases examined, the alkyne is oriented parallel to one edge of the trimetallic framework but the particular location varies. In the iron complex $CpNiCoFe(CO)_6(C_2Et_2)$ (**1b**), it is parallel to the Ni–Co edge and all carbonyls are terminal. In the ruthenium and osmium complexes $CpNiCoRu(CO)_6(C_2Ph_2)$ (**2a**) and $CpNiCoOs(CO)_6C_2Ph_2$ (**3a**), the orientation is parallel to the Ni–Ru or Ni–Os edge and one of the CO groups adopts a semibridging position across the Co–Ru or Co–Os bond. A similar arrangement is observed in an iron complex when one of the carbonyl groups bound to cobalt is replaced by triphenylphosphine to give $CpNiCoFe(CO)_5(PPh_3)(C_2Ph_2)$ (**1d**). Crystal data: **1b**, monoclinic, $P2_1/n$, a = 9.559 (3) Å, b = 12.573 (5) Å, c = 16.175 (4) Å, β = 104.42 (3)°, Z = 4, V = 1883 Å^3, λ(Mo Kα_1) = 0.709 30 Å, μ(Mo Kα) = 26.4 cm^{-1}, d_{calcd} = 1.72 g cm^{-3}, d_{measd} = 1.74 g cm^{-3}, R = 0.029 and R_w = 0.033 for 1387 observed reflections, with $I \geq 2.3\sigma(I)$ (1748 measured with 40° ≥ 2θ ≥ 3°); **1d**, monoclinic, $P2_1/c$, a = 11.698 (2) Å, b = 14.768 (3) Å, c = 22.616 (4) Å, β = 111.82 (1)°, Z = 4, V = 3627 Å^3, λ(Mo Kα_1) = 0.709 30 Å, μ(Mo Kα) = 14.7 cm^{-1}, d_{calcd} = 1.48 g cm^{-3}, d_{measd} = 1.51 g cm^{-3}, R = 0.057 and R_w = 0.070 for 1109 observed reflections, with $I \geq 2.3\sigma(I)$ (2316 measured with 35° ≥ 2θ ≥ 3°); **2a**, monoclinic, $P2_1/c$, a = 9.964 (2) Å, b = 9.5112 (6) Å, c = 24.835 (2) Å, β = 90.11 (1)°, Z = 4, V = 2353 Å^3, λ(Mo Kα_1) = 0.709 30 Å, μ(Mo Kα) = 21.7 cm^{-1}, d_{calcd} = 1.78 g cm^{-3}, d_{measd} = 1.80 g cm^{-3}, R = 0.036 and R_w = 0.042 for 1816 observed reflections with $I \geq 2.3\sigma(I)$ (3100 measured with 45° ≥ 2θ ≥ 3.5°); **3a**, monoclinic, $P2_1/c$, a = 9.950 (2) Å, b = 9.505 (2) Å, c = 24.813 (4) Å, β = 90.10 (3)°, Z = 4, V = 2347 Å^3, λ(Mo Kα_1) = 0.70930 Å, μ(Mo Kα) = 69.4 cm^{-1}, d_{calcd} = 2.03 g cm^{-3}, d_{measd} = 2.11 g cm^{-3}, R = 0.033 and R_w = 0.039 for 2503 reflections with $I \geq 2.3\sigma(I)$ (3063 measured with 45° ≥ 2θ ≥ 3°). The variable-temperature ^{1}H NMR spectra of **1c** (Fe), **2c** (Ru), and **3c** (Os), containing the unsymmetrical alkyne MeC_2Ph, indicate that the clusters are nonrigid and the alkyne substituents interchange position by rotation of the alkyne moiety on the face of the metal triangle. Examination of the C_2Et_2 complexes shows this to be nondissociative and to involve no transfer from one face of the metal triangle to the other.

Introduction

Alkynes provide great structural and chemical diversity in their interactions with transition metals in complexes. One aspect of current interest is their ability to bind simultaneously to three or four transition metals in clusters, and these compounds have recently been reviewed.[1,2] Somewhat different viewpoints have been adopted in describing what constitutes the "cluster" in these compounds. To cite the trimetallic case, the alkyne may simply be viewed as one ligand among others binding to a triangular M_3 cluster.[3] Alternatively, the alkyne carbon atoms may be considered to be an integral part of a M_3C_2 five-vertex cluster polyhedron.[4]

The M_3C_2 clusters adopt two distinct geometries that differ in the orientation of the alkyne C_2 vector with respect to the M_3 triangle. In the first, this vector is parallel to a metal–metal edge, and in this structure, the alkyne may be designated[5] as η^2-||; the polyhedron is a *nido*-M_3C_2 cluster with a square-based-pyramidal

(1) Sappa, E.; Tiripicchio, A.; Braunstein, P. *Chem. Rev.* **1983**, *83*, 203; *Coord. Chem. Rev.* **1985**, *65*, 219.
(2) Bruce, M. I. *J. Organomet. Chem.* **1983**, *257*, 417.
(3) Schilling, B. E. R.; Hoffmann, R. *J. Am. Chem. Soc.* **1979**, *101*, 3456.
(4) Halet, J. F.; Saillard, J. Y.; Lissillour, R.; McGlinchey, M.; Jaouen, G. *Inorg. Chem.* **1985**, *24*, 218.
(5) Thomas, M. G.; Muetterties, E. L.; Day, R. O.; Day, V. W. *J. Am. Chem. Soc.* **1976**, *98*, 4645.

0020-1669/86/1325-1631$01.50/0

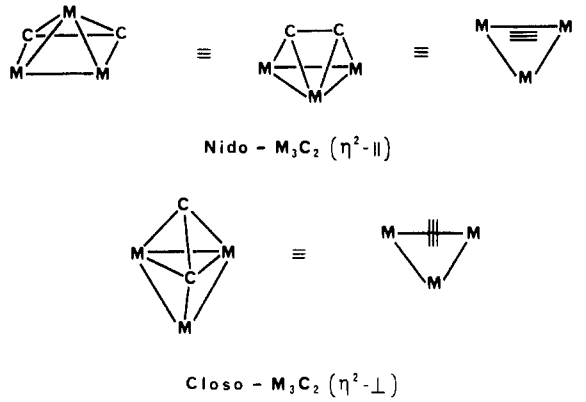

Figure 1. Depictions of *nido*- and *closo*-M_3C_2 clusters.

geometry and seven skeletal electron pairs. In the second, the vector is perpendicular to a metal–metal edge (η^2-⊥)[5] and the polyhedron is a *closo*-M_3C_2 cluster with a trigonal-bipyramidal geometry and six skeletal electron pairs (Figure 1).

The available X-ray structures up to 1984 for some 24 homo- and heterotrimetallic alkyne clusters have been reviewed, and the nido structure is notably the more common.[4] In *hetero*trimetallic clusters, there emerges the question as to which of several possible isomers will be favored; i.e., which edge will be the one parallel or perpendicular to which the alkyne will be oriented in the closo or nido structure.

The majority of heterotrimetallic alkyne clusters contain only two different metals. Other than those described in this paper, the only ones known to us to contain three different metals are those built from CpNi and $Fe(CO)_3$, with either $Co(CO)_3$ or $Mo(CO)_2Cp$ as the third vertex.[6] We were interested in examining a series of such clusters, in which one of the metals is varied down a group, in case there were structural changes. For this purpose, we chose the compounds $CpNiCoM(CO)_6(C_2RR')$ [M = Fe (**1**), Ru (**2**), or Os (**3**)], where the clusters are built from CpNi, $Co(CO)_3$, and $M(CO)_3$ fragments. A FeCoNi phosphine-substituted cluster, $CpNiCoFe(CO)_5(PPh_3)(C_2Ph_2)$ (**1d**), in which $Co(CO)_3$ is replaced by $Co(CO)_2(PPh_3)$, was also examined, and a preliminary report of this has been published.[7] The clusters were synthesized by the addition of a $M(CO)_3$ fragment to the heterobinuclear complex[8] $CpNiCo(CO)_3C_2RR'$ (**4**), which in turn was obtainable from Cp_2Ni and $Co_2(CO)_6(C_2RR')$ (**5**).

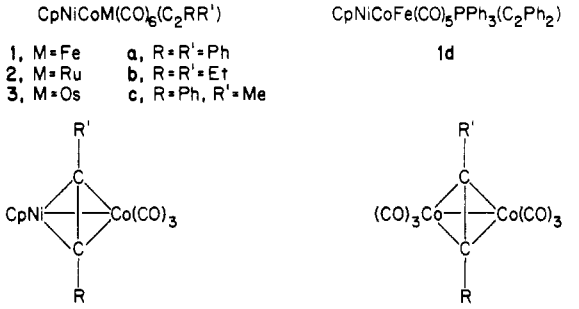

4a, R=Ph, R'=Ph
b, R=Et, R'=Et
c, R=Ph, R'=Me

5a, R=Ph, R'=Ph
b, R=Et, R'=Et
c, R=Ph, R'=Me

Experimental Section

General Procedures. $CpNiCo(CO)_3(C_2RR')$ (**4**: R = R' = Ph, Et; R = Ph, R' = Me),[8] $Fe_2(CO)_9$,[9] and $Ru(CO)_5$[10] were prepared according to literature methods. The photochemical synthesis of $Fe_2(CO)_9$ was performed in a 250-mL Pyrex vessel equipped with a water-cooled quartz finger that held a 200-W Hanovia high-pressure mercury UV source. Nitrogen was passed through the reaction vessel prior to the addition of solvent and starting material, and slow passage of nitrogen was maintained during the reaction. $Os_3(CO)_{12}$ and $Os(CO)_5$[10] were kindly supplied by Dr. R. K. Pomeroy of this department. Diphenylacetylene (Aldrich), 3-hexyne (Columbia Organic), and phenylmethylacetylene (Aldrich) were used as received. All solvents were dried by standard methods and distilled under nitrogen. Reactions were carried out in Schlenkware, connected to a switchable inert-atmosphere or vacuum supply, and were conducted under nitrogen.

Infrared spectra were recorded on a Perkin-Elmer 983 spectrophotometer. ^1H NMR spectra were recorded on a Varian XL100 and by M. M. Tracey on a Bruker WM400 instrument at 100 and 400 MHz, respectively. All nuclear Overhauser enhancement and spin-saturation-transfer experiments were performed on the Bruker WM400. Mass spectral analyses were carried out by G. Owen on a Hewlett-Packard 5985 system operating at 70 eV. Microanalyses were performed by M. K. Yang of the microanalytical laboratory at Simon Fraser University.

Preparation of $CpNiCoFe(CO)_6(C_2RR')$ (1a, R = R' = Ph; 1b, R = R' = Et; 1c, R = Ph, R' = Me). A large excess of $Fe_2(CO)_9$ and the corresponding heterobimetallic alkyne compound $CpNiCo(CO)_3(C_2RR')$ (**4**: R = R' = Ph, Et; R = Ph, R' = Me) (typically in the range of 0.1–0.2 g) were stirred overnight at room temperature in approximately 30 mL of hexane. The solvent was removed in vacuo. Fresh hexane (6–8 mL) was added and the solution chromatographed on a Florisil column. $Fe_3(CO)_{12}$ and the starting heterobimetallic alkyne were eluted with hexane; then, with hexane/CH_2Cl_2 (5:1) a dark green or light brown band was recovered and identified as the appropriate heterotrimetallic alkyne $CpNiCoFe(CO)_6(C_2RR')$. Yields were variable but typically ranged from 30 to 60%. **1a** gave inexplicably high (but reproducible) analyses. Anal. Calcd for $CpNiCoFe(CO)_6(C_2Ph_2)$ (**1a**): C, 51.33; H, 2.59. Found: C, 52.06, 52.18, 52.19; H, 3.62, 3.63, 3.75. Calcd for $CpNiCoFe(CO)_6(C_2Et_2)$ (**1b**): C, 41.77; H, 3.09. Found: C, 41.87; H, 3.12.

Preparation of $CpNiCoRu(CO)_6(C_2RR')$ (2a, R = R' = Ph; 2b, R = R' = Et; 2c, R = Ph, R' = Me). In a typical reaction, $CpNiCo(CO)_3(C_2RR')$ (**4**: R = R' = Ph, Et; R = Ph, R' = Me) (0.1–0.2 g) and excess $Ru(CO)_5$ were added to 25 mL of hexane, and the resulting mixture was stirred at room temperature until the absorptions from $Ru(CO)_5$ (ν(CO) = 2039, 2004 cm^{-1}) disappeared. This usually required about 18 h. The temperature could be increased to 40–45 °C to decrease the reaction time without affecting the yield, but more $Ru_3(CO)_{12}$ was formed as a result. After the reaction was complete, the solvent and any excess $Ru(CO)_5$ were removed in vacuo and the residue was dissolved in the minimum amount of hexane. Column chromatography on Florisil with hexane as eluant yielded $Ru_3(CO)_{12}$ as a yellow band followed by residual $CpNiCo(CO)_3(C_2RR')$. The product $CpNiCoRu(CO)_6(C_2RR')$ was then eluted with hexane/CH_2Cl_2 (4:1) as a brown band in 10–15% yield. Anal. Calcd for $CpNiCoRu(CO)_6(C_2Ph_2)$ (**2a**): C, 47.65; H, 2.51. Found: C, 47.82; H, 2.39. Calcd for $CpNiCoRu(CO)_6(C_2Et_2)$ (**2b**): C, 38.23; H, 2.83. Found: C, 38.18; H, 2.79.

Preparation of $CpNiCoOs(CO)_6(C_2RR')$ (3a, R = R' = Ph; 3b, R = R' = Et; 3c, R = Ph, R' = Me). $CpNiCo(CO)_3(C_2RR')$ (R = R' = Ph, Et; R = Ph, R' = Me) and excess $Os(CO)_5$ were added to 25 mL of hexane, and the mixture was heated to 40–45 °C for 10–12 h. The volume was reduced to 5 mL and the solution chromatographed on a Florisil column, and variable, but usually small, amounts of $Os_3(CO)_{12}$ were first eluted with hexane followed by a green band of residual $CpNiCo(CO)_3(C_2RR')$. With use of a hexane/$CHCl_3$ (5:1) mixture, the product $CpNiCoOs(CO)_6(C_2RR')$ was next eluted as a dark brown band. Anal. Calcd for $CpNiCoOs(CO)_6(C_2Ph_2)$ (**3a**): C, 41.75; H, 2.10. Found: C, 41.79; H, 2.20. Calcd for $CpNiCoOs(CO)_6(C_2Et_2)$ (**3b**): C, 32.76; H, 2.43. Found: C, 32.87; H, 2.49.

Preparation of $CpNiCoFe(CO)_5(PPh_3)(C_2Ph_2)$ (1d). Compound **1a** (0.12 g, 0.21 mmol) and PPh_3 (0.07 g, 0.27 mmol) were added to 20 mL of hexanes, and the mixture was stirred for 12 h. The volume was reduced to 4–5 mL followed by chromatography on Florisil. Elution with CH_2Cl_2/hexane yielded a black band from which **1d** was obtained as a dark brown solid in 90% yield. Anal. Calcd for $CpNiCoFe(CO)_5(PPh_3)(C_2Ph_2)$: C, 61.58; H, 3.69. Found: C, 62.21; H, 4.40.

NMR Determination of Exchange Kinetics and Activation Energies. The exchange kinetics for the ^1H NMR resonances of the ethyl groups in the complex $CpNiCoFe(CO)_6(C_2Et_2)$ (**1b**) were followed by observing the transfer of magnetization between the magnetically inequivalent

(6) (a) Jaouen, G.; Marinetti, A.; Mentzen, R.; Mutin, R.; Saillard, J. Y.; Sayer, B. G.; McGlinchey, M. J. *Organometallics* **1982**, *1*, 753. (b) Mlekuz, M.; Bougeard, P.; Sayer, B. G.; Peng, S.; McGlinchey, M. J.; Marinetti, A.; Saillard, J. Y.; Naceur, J. B.; Mentzen, B.; Jaouen, G. *Organometallics* **1985**, *4*, 1123.
(7) Einstein, F. W. B.; Freeland, B. H.; Tyers, K. G.; Sutton, D.; Waterous, J. M. *J. Chem. Soc., Chem. Commun.* **1982**, 371.
(8) Freeland, B. H.; Hux, J. E.; Payne, N. C.; Tyers, K. G. *Inorg. Chem.* **1980**, *19*, 693.
(9) Braye, E. H.; Hübel, W. *Inorg. Synth.* **1966**, *8*, 178.
(10) Rushman, P.; van Buuren, G. N.; Shiralian, M.; Pomeroy, R. K. *Organometallics* **1983**, *2*, 693.

Table I. Summary of Crystal Data for $CpNiCoFe(CO)_5(PPh_3)(C_2Ph_2)$ (**1d**), $CpNiCoRu(CO)_6(C_2Ph_2)$ (**2a**), $CpNiCoOs(CO)_6(C_2Ph_2)$ (**3a**), and $CpNiCoFe(CO)_6(C_2Et_2)$ (**1b**)

	1d	2a	3a	1b
mol wt	819.15	630.1	719.3	488.8
space group	$P2_1/c$	$P2_1/c$	$P2_1/c$	$P2_1/n$
a, Å	11.698 (2)	9.964 (2)	9.950 (2)	9.559 (3)
b, Å	14.768 (3)	9.5112 (6)	9.505 (2)	12.573 (5)
c, Å	22.616 (4)	24.835 (2)	24.813 (4)	16.175 (4)
β, deg	111.82 (1)	90.11 (1)	90.10 (3)	104.42 (3)
Z	4	4	4	4
cell vol, Å^3	3627	2353	2347	1883
ρ(calcd), g cm^{-3}	1.48	1.78	2.03	1.72
ρ(obsd), g cm^{-3}	1.51	1.80	2.11	1.74
μ(Mo Kα), cm^{-1}	14.7	21.7	69.4	26.4
total no. of reflcns measd	2316	3100	3063	1748
no. of reflcns with $I \geq 2.3\sigma(I)$	1109	1816	2503	1387
2θ data limits, deg	3, 35	3.5, 45	3, 45	3, 40
final R	0.057	0.036	0.033	0.029
final R_w	0.070	0.042	0.039	0.033
GOF	1.32	1.37	1.52	1.23

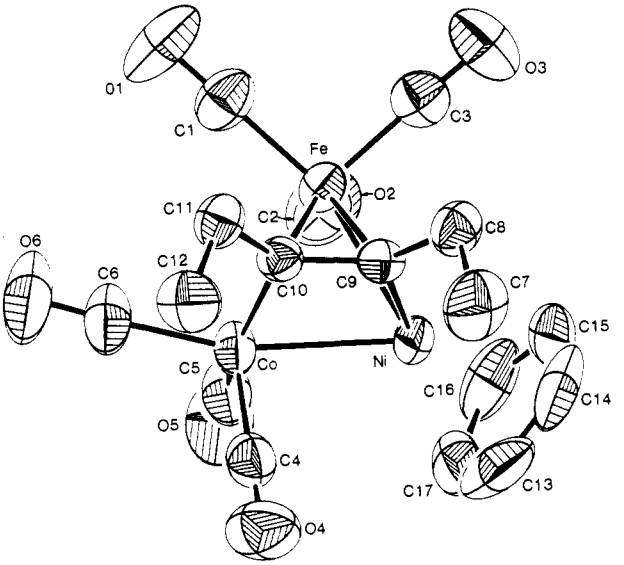

Figure 2. Structure of $CpNiCoFe(CO)_6(C_2Et_2)$ (**1b**).

methyl groups in a modification of the Forsén–Hoffmann technique.[11] A selective 180° pulse was applied to invert one methyl resonance, and after a variable delay time a normal 90° observation pulse was applied. The second methyl resonance decreased in intensity as a result of the exchange and consequent magnetization transfer, and this is revealed in a difference spectrum. This was performed at five different temperatures: 291, 300, 307, 314, and 321 K. It was not possible to repeat the experiment for Ru and Os compounds **2b** and **3b** owing to the smaller chemical shift separation of the methyl resonances. The kinetic parameters for **1c**, **2c**, and **3c** were obtained from the coalescence temperatures for the Cp or Me resonance. The $\Delta\nu_\infty$ values used were those obtained for the separation of the two methyl or Cp resonances at 243 K.

X-ray Structure Determinations. All data were collected on an Enraf-Nonius CAD-4 or Picker FACS-1 diffractometer using Mo Kα radiation [λ(Mo Kα_1) = 0.709 30 Å]. A summary of the crystal data for the structures of **1b**, **1d**, **2a**, and **3a** is given in Table I. Additional details relating to each structure determination are as follows.

(a) $CpNiCoFe(CO)_3(C_2Et_2)$ (1b). A dark green needle, 0.07 mm × 0.12 mm × 0.36 mm, was recrystallized from hexane/$CHCl_3$ at 0 °C and was used for the diffraction studies. Data were collected at a scan speed varying from 0.3 to 5.0° min^{-1} plus dispersion correction above and below Kα_1. Two standard reflections were monitored every 150 reflections and showed no indication of intensity loss. Absorption corrections were applied via an empirical correction (ψ scans; transmission factors varied from 0.72 to 0.84). The metal atoms were located by MULTAN, and the non-hydrogen atoms, from a series of difference Fourier syntheses and least-squares refinement. The hydrogen atom positions in this and the following structures were calculated geometrically with d(C–H) = 0.98 Å, given isotropic thermal parameters equal to those of the carbon atom to which they were attached, and were included as fixed contributions in further refinement. All non-hydrogen atoms were refined anisotropically. The largest peak in a final difference map, 0.6 (2) e Å^{-3}, was located between the Ni atom and the Cp ring. Atomic coordinates are listed in Table II, and bond distances and angles, in Table III. An ORTEP diagram with the atom-labeling scheme is shown in Figure 2.

(b) $CpNiCoFe(CO)_5(PPh_3)(C_2Ph_2)$ (1d). A black crystal, 0.09 mm × 0.11 mm × 0.15 mm, was obtained from hexane/$CHCl_3$. Preliminary Weissenberg and precession photographs indicated the crystal to be monoclinic, and systematic absences ($0k0$, $k = 2n + 1$; $h0l$, $l = 2n + 1$) defined the space group as $P2_1/c$. Data were collected at a scan rate of 2° min^{-1} for $3° \leq 2\theta \leq 35°$ with a symmetrical scan width of (1.2 + 0.692 tan θ)°. There were very few observed reflections beyond 35°, so the data collection was terminated at that point. Two standards were measured every 70 reflections and showed only random fluctuations. Absorption corrections were applied by using an analytical correction (transmission factors 0.75–0.86). The positions of the metal atoms and the phosphorus atom were located by MULTAN, and the non-hydrogen atoms, from a series of difference Fourier syntheses and least-squares refinement. The metal atoms and the phosphorus atom were refined

Table II. Atom Coordinates (×10^4) for $CpNiCoFe(CO)_6(C_2Et_2)$ (**1b**)

	x	y	z
Ni	1867.4 (8)	2196.5 (6)	937.7 (5)
Co	3918.4 (9)	3390.7 (6)	1366.1 (5)
Fe	3296.0 (9)	2527.4 (7)	−64.1 (6)
C(1)	4719 (7)	2952 (6)	−505 (4)
O(1)	5660 (6)	3210 (5)	−777 (4)
C(2)	2036 (7)	3553 (5)	−495 (4)
O(2)	1231 (5)	4199 (4)	−788 (3)
C(3)	2593 (7)	1559 (5)	−849 (4)
O(3)	2130 (6)	918 (4)	−1342 (3)
C(4)	4010 (7)	3027 (5)	2444 (4)
O(4)	4060 (5)	2773 (4)	3123 (3)
C(5)	2692 (7)	4508 (5)	1199 (4)
O(5)	1950 (5)	5223 (4)	1111 (4)
C(6)	5556 (7)	4116 (5)	1432 (5)
O(6)	6615 (6)	4537 (4)	1461 (4)
C(7)	3759 (8)	−336 (5)	1648 (5)
C(8)	3509 (7)	202 (5)	800 (4)
C(9)	3512 (6)	1400 (4)	857 (4)
C(10)	4687 (6)	2060 (4)	1045 (3)
C(11)	6270 (6)	1754 (5)	1219 (4)
C(12)	6989 (7)	1638 (6)	2154 (4)
C(13)	605 (8)	1833 (8)	1778 (5)
C(14)	291 (8)	1128 (6)	1122 (6)
C(15)	−252 (7)	1694 (7)	388 (5)
C(16)	−312 (7)	2729 (6)	575 (5)
C(17)	219 (8)	2813 (6)	1443 (6)

Table III. Bond Distances (Å) and Angles (deg) for $CpNiCoFe(CO)_6(C_2Et_2)$ (**1b**)

Ni–Co	2.432 (1)	Ni–C(9)	1.898 (5)
Ni–Fe	2.402 (1)	C(1)–O(1)	1.144 (7)
Co–Fe	2.494 (1)	C(2)–O(2)	1.140 (7)
Fe–C(1)	1.767 (6)	C(3)–O(3)	1.144 (7)
Fe–C(2)	1.786 (6)	C(4)–O(4)	1.137 (7)
Fe–C(3)	1.773 (6)	C(5)–O(5)	1.133 (7)
Fe–C(9)	2.036 (5)	C(6)–O(6)	1.134 (7)
Fe–C(10)	2.037 (5)	C(7)–C(8)	1.492 (9)
Co–C(4)	1.781 (6)	C(8)–C(9)	1.510 (7)
Co–C(5)	1.811 (6)	C(9)–C(10)	1.371 (7)
Co–C(6)	1.791 (6)	C(10)–C(11)	1.522 (7)
Co–C(10)	1.953 (5)	C(11)–C(12)	1.507 (8)
Ni–Cp(ctr)	1.750 (4)		
Ni–Co–Fe	58.36 (3)	Co–C(5)–O(5)	178.2 (5)
Ni–Fe–Co	59.52 (3)	Co–C(6)–O(6)	177.0 (6)
Fe–Ni–Co	62.11 (3)	Ni–C(9)–C(10)	108.0 (4)
Fe–C(1)–O(1)	178.2 (6)	Ni–C(9)–Fe	75.2 (2)
Fe–C(2)–O(2)	178.2 (6)	Co–C(10)–C(9)	103.9 (4)
Fe–C(3)–O(3)	178.4 (5)	Co–C(10)–Fe	77.3 (2)
Co–C(4)–O(4)	178.3 (5)		

(11) Dahlquist, F. W.; Longmuir, K. J.; DuVernet, R. B. *J. Magn. Reson.* **1975**, *17*, 406.

Table IV. Atom Coordinates ($\times 10^4$) for $CpNiCoFe(CO)_5(PPh_3)(C_2Ph_2)$ (**1d**)

	x	y	z
Co	6468.4 (26)	2282.0 (20)	4855.4 (13)
Fe	7936.3 (28)	1045.6 (20)	5340.0 (14)
Ni	6941.6 (26)	1930.5 (19)	5952.7 (12)
P	6075 (5)	2673 (4)	3846 (3)
C(1)	7443 (22)	37 (16)	5515 (11)
C(2)	8533 (20)	535 (15)	4947 (10)
C(3)	9199 (19)	1057 (15)	6019 (10)
C(4)	6134 (19)	1136 (15)	4704 (10)
C(5)	5137 (21)	2693 (16)	4875 (11)
O(1)	7263 (14)	-729 (11)	5629 (7)
O(2)	8808 (14)	166 (10)	4434 (7)
O(3)	10120 (14)	1060 (11)	6498 (7)
O(4)	5410 (13)	567 (11)	4428 (7)
O(5)	4263 (13)	3037 (10)	4888 (7)
C(6)	8342 (15)	2380 (12)	5312 (8)
C(7)	7782 (15)	2827 (12)	5642 (8)
C(11)	6900 (18)	1972 (14)	3445 (9)
C(12)	6270 (18)	1219 (15)	3100 (10)
C(13)	7038 (20)	678 (16)	2865 (10)
C(14)	8168 (21)	827 (16)	2977 (11)
C(15)	8776 (20)	1562 (16)	3288 (10)
C(16)	8097 (18)	2156 (14)	3564 (9)
C(21)	4509 (17)	2596 (13)	3296 (9)
C(22)	4083 (20)	2991 (16)	2705 (10)
C(23)	2858 (21)	2926 (16)	2300 (11)
C(24)	2020 (21)	2458 (17)	2461 (11)
C(25)	2393 (21)	2019 (17)	3024 (11)
C(26)	3645 (19)	2082 (15)	3439 (10)
C(31)	6440 (17)	3809 (13)	3712 (8)
C(32)	6763 (18)	4148 (13)	3220 (9)
C(33)	6914 (20)	5074 (15)	3141 (11)
C(34)	6772 (20)	5698 (15)	3556 (10)
C(35)	6406 (19)	5401 (14)	4034 (9)
C(36)	6243 (19)	4484 (15)	4128 (10)
C(41)	9328 (16)	2751 (13)	5102 (8)
C(42)	9276 (16)	3615 (13)	4883 (8)
C(43)	10171 (17)	3958 (13)	4667 (9)
C(44)	11138 (19)	3408 (15)	4690 (10)
C(45)	11230 (20)	2555 (15)	4906 (10)
C(46)	10349 (19)	2225 (15)	5135 (10)
C(51)	8062 (15)	3697 (12)	5978 (8)
C(52)	7108 (17)	4293 (13)	5952 (9)
C(53)	7473 (19)	5137 (14)	6303 (10)
C(54)	8621 (20)	5327 (15)	6636 (10)
C(55)	9543 (18)	4773 (13)	6665 (9)
C(56)	9270 (17)	3966 (13)	6328 (9)
C(61)	7542 (21)	1502 (18)	6891 (11)
C(62)	6437 (19)	979 (14)	6487 (10)
C(63)	5481 (22)	1538 (17)	6266 (11)
C(64)	5826 (22)	2376 (17)	6482 (12)
C(65)	7081 (19)	2324 (16)	6857 (10)

anisotropically. The largest peak in a final difference map, 0.43 (20) e $Å^{-3}$, was located near C(61) of the aromatic ring. Atomic coordinates are listed in Table IV, and bond distances and angles, in Table V. An ORTEP diagram with the atom-labeling scheme is shown in Figure 3.

(c) $CpNiCoRu(CO)_6(C_2Ph_2)$ (2a). A dark brown crystal, 0.11 mm × 0.19 mm × 0.24 mm, obtained from a hexane solution was chosen for the diffraction studies. Preliminary Weissenberg and precession photographs indicated the crystal to be monoclinic, space group $P2_1/c$. Data were collected at a scan rate of 2° min^{-1} for $3° \le 2\theta \le 45°$ with a symmetrical scan width of $(1.4 + 0.692 \tan \theta)°$. Two standards were measured after every 70 reflections but showed only random fluctuations. Absorption corrections were applied by using an analytical correction (transmission factors 0.64–0.79). The metal atoms were located by MULTAN, and the non-hydrogen atoms, from a series of difference Fourier syntheses and least-squares refinement. The metal atoms, carbonyl ligands, and cyclopentadienyl ligand were refined anisotropically. The largest peak in a final difference map, 0.53 (22) e $Å^{-3}$, was located between the Ru atom and the nearest phenyl ring. Atomic coordinates are given in Table VI, and bond distances and angles, in Table VII. An ORTEP diagram with the atom-labeling scheme is shown in Figure 4.

(d) $CpNiCoOs(CO)_6(C_2Ph_2)$ (3a). A triangular, platelike dark brown crystal, 0.49 mm × 0.50 mm × 0.60 mm × 0.06 mm, obtained from a hexane/CH_2Cl_2 solution at −20 °C, was chosen for the diffraction studies. Data were collected with a variable scan speed of 0.8–5.0° min^{-1} for reflections with $3.0° \le 2\theta \le 45°$. The scan width was 0.7° plus dispersion correction above and below $K\alpha_1$ for $3° \le 2\theta \le 40°$ and 0.9° plus

Table V. Bond Distances (Å) and Angles (deg) for $CpNiCoFe(CO)_5(PPh_3)(C_2Ph_2)$ (**1d**)

Ni–Co	2.390 (4)	Co–C(7)	2.04 (2)
Ni–Fe	2.486 (4)	C(6)–C(7)	1.34 (2)
Fe–Co	2.467 (4)	C(6)–C(41)	1.50 (2)
Co–P	2.230 (6)	C(7)–C(51)	1.47 (2)
Fe–C(1)	1.70 (2)	C(1)–O(1)	1.20 (3)
Fe–C(2)	1.79 (2)	C(2)–O(2)	1.13 (3)
Fe–C(3)	1.69 (2)	C(3)–O(3)	1.21 (3)
Fe–C(4)	2.07 (2)	C(4)–O(4)	1.19 (3)
Co–C(4)	1.74 (2)	C(5)–O(5)	1.15 (3)
Co–C(5)	1.69 (2)	Ni–Cp(ctr)	1.75 (1)
Fe–C(6)	2.03 (2)	P–C(11)	1.86 (2)
Ni–C(7)	1.93 (2)	P–C(21)	1.80 (2)
Co–C(6)	2.05 (2)	P–C(31)	1.79 (2)
Ni–Co–Fe	61.55 (12)	Co–C(5)–O(5)	175 (2)
Co–Fe–Ni	57.71 (11)	Ni–C(7)–Co	74.1 (6)
Co–Ni–Fe	60.74 (11)	Fe–C(6)–Co	74.3 (6)
Fe–Co–P	119.4 (2)	Ni–C(7)–C(6)	107 (1)
Ni–Co–P	177.2 (2)	Ni–C(7)–C(51)	117 (1)
Fe–C(1)–O(1)	170 (2)	Fe–C(6)–C(7)	107 (1)
Fe–C(2)–O(2)	173 (2)	Fe–C(6)–C(41)	125 (1)
Fe–C(3)–O(3)	179 (2)	C(6)–C(7)–C(51)	131 (1)
Fe–C(4)–O(4)	131 (2)	C(7)–C(6)–C(41)	126 (1)
Co–C(4)–O(4)	148 (2)		

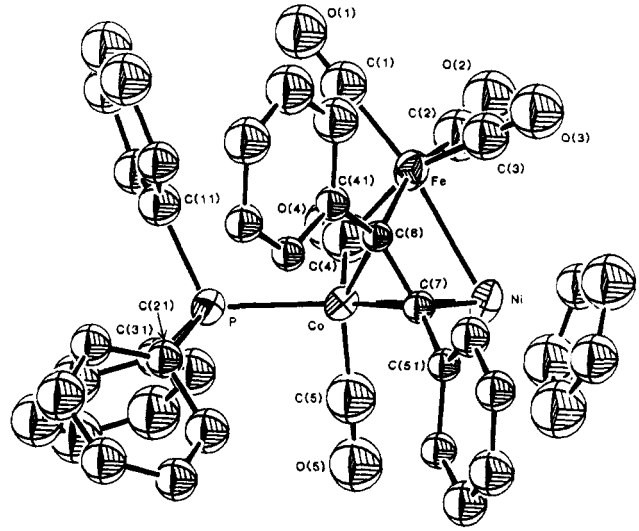

Figure 3. Structure of $CpNiCoFe(CO)_5(PPh_3)(C_2Ph_2)$ (**1d**).

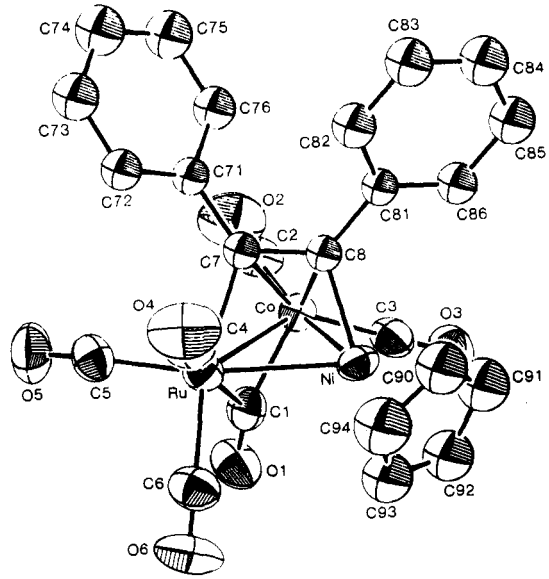

Figure 4. Structure of $CpNiCoRu(CO)_6(C_2Ph_2)$ (**2a**).

Table VI. Atom Coordinates ($\times 10^4$) for $CpNiCoRu(CO)_6(C_2Ph_2)$ (**2a**)

	x	*y*	*z*
Ni	3775.9 (9)	2816.8 (11)	913.4 (4)
Co	1963.9 (10)	4470.4 (11)	969.6 (4)
Ru	1484.3 (7)	2061.6 (7)	546.4 (2)
C(1)	1639 (8)	4291 (8)	248 (3)
O(1)	1579 (6)	4819 (6)	9829 (2)
C(2)	609 (9)	5620 (9)	1144 (3)
O(2)	−220 (7)	6384 (7)	1256 (3)
C(3)	3272 (9)	5708 (9)	943 (3)
O(3)	4053 (7)	6567 (7)	923 (2)
C(4)	1738 (9)	197 (9)	818 (3)
O(4)	1917 (8)	−878 (6)	985 (3)
C(5)	−386 (9)	1895 (9)	386 (3)
O(5)	−1496 (6)	1806 (7)	285 (3)
C(6)	2040 (10)	1644 (9)	−186 (3)
O(6)	2366 (8)	1412 (8)	−612 (2)
C(7)	1304 (7)	2669 (7)	1367 (3)
C(8)	2606 (7)	2967 (8)	1516 (3)
C(71)	132 (7)	2538 (7)	1730 (3)
C(72)	−667 (8)	1357 (8)	1694 (3)
C(73)	−1716 (9)	1125 (10)	2062 (3)
C(74)	−1943 (9)	2113 (10)	2462 (10)
C(75)	−1156 (9)	3281 (9)	2504 (3)
C(76)	−115 (8)	3514 (8)	2136 (3)
C(81)	3194 (7)	3043 (8)	2066 (3)
C(82)	4167 (8)	4011 (8)	2196 (3)
C(83)	4754 (9)	4043 (9)	2714 (3)
C(84)	4308 (9)	3117 (9)	3091 (3)
C(85)	3363 (9)	2152 (10)	2981 (3)
C(86)	2772 (8)	2077 (9)	2462 (3)
C(91)	4951 (9)	7196 (12)	4712 (3)
C(92)	4971 (10)	6205 (11)	4310 (5)
C(93)	4461 (9)	6806 (12)	3846 (4)
C(94)	4128 (9)	8154 (12)	3954 (4)
C(95)	4434 (9)	8392 (10)	4508 (4)

Table VII. Bond Distances (Å) and Angles (deg) for $CpNiCoRu(CO)_6(C_2Ph_2)$ (**2a**)

Ni–Ru	2.560 (1)	Ru–C(7)	2.126 (7)
Ni–Co	2.399 (1)	Ni–Cp(ctr)	1.747 (1)
Co–Ru	2.565 (1)	Ni–C(8)	1.903 (7)
Co–C(1)	1.828 (8)	C(7)–C(71)	1.480 (10)
Co–C(2)	1.791 (9)	C(7)–C(8)	1.377 (9)
Co–C(3)	1.758 (8)	C(8)–C(81)	1.489 (9)
Co–C(7)	2.085 (7)	C(1)–O(1)	1.158 (9)
O–C(8)	2.071 (7)	C(2)–O(2)	1.135 (10)
Ru–C(1)	2.251 (8)	C(3)–O(3)	1.129 (10)
Ru–C(4)	1.913 (9)	C(4)–O(4)	1.118 (10)
Ru–C(5)	1.912 (9)	C(5)–O(5)	1.135 (10)
Ru–C(6)	1.943 (8)	C(6)–O(6)	1.130 (10)
Ni–Co–Ru	61.98 (4)	Ru–C(5)–O(5)	179.1 (8)
Ni–Ru–Co	55.82 (4)	Ru–C(6)–O(6)	179.5 (8)
Ru–Ni–Co	62.21 (4)	Ru–C(7)–Co	75.0 (2)
Co–C(1)–O(1)	148.2 (7)	Ru–C(7)–C(8)	103.4 (5)
Co–C(1)–Ru	77.2 (3)	Ni–C(8)–Co	74.1 (2)
Co–C(2)–O(2)	177.7 (8)	Ni–C(8)–C(7)	110.6 (5)
Co–C(3)–O(3)	175.7 (8)	Co–Ru–C(1)	44.0 (2)
Ru–C(1)–O(1)	134.5 (6)	Ru–Co–C(1)	58.8 (3)
Ru–C(4)–O(4)	178.1 (8)		

dispersion correction for $40° \leq 2\theta \leq 45°$. Two standards were measured every 150 reflections but showed only random fluctuations. Absorption corrections were applied via an analytical correction (transmission factors 0.23–0.66). The positions of the metal atoms were located by MULTAN, and non-hydrogen atoms, from a series of difference Fourier syntheses and least-squares refinement. All the non-hydrogen atoms were refined anisotropically. The largest peak in a final difference map, 1.1 (2) e Å^{-3}, was 1.2 Å from the Os atom and 0.8 Å from C(3) and was of no chemical significance. Atomic coordinates are given in Table VIII; bond distances and angles, in Table IX. A labeled ORTEP diagram is shown in Figure 5.

Results and Discussion

Synthesis. $CpNiCo(CO)_3(C_2RR')$ (**1a**, R = R′ = Ph; **4b**, R = R′ = Et; **4c**, R = Ph, R′ = Me) can be synthesized in reasonable yield from Cp_2Ni and $Co_2(CO)_6(C_2RR')$ (**5a–c**), the latter obtainable from the reaction of $Co_2(CO)_8$ and C_2RR'. Compounds **4a–c** are air-stable, both in the solid state and in solution, and are purified easily by column chromatography.[8]

The reactions of excess $Fe_2(CO)_9$ with $CpNiCo(CO)_3(C_2RR')$ (**4a–c**) in hexanes produced in reasonable yield (≈25–30%) the heterotrimetallic alkyne clusters $CpNiCoFe(CO)_6(C_2Ph_2)$ (**1a**), $CpNiCoFe(CO)_6(C_2Et_2)$ (**1b**), and $CpNiCoFe(CO)_6(MeC_2Ph)$ (**1c**), which were separated from residual starting materials and small amounts of other products by column chromatography. This always included some $Fe_3(CO)_{12}$, the formation of which was increased at higher reaction temperatures.

The effects of varying the conditions were studied by using the $Fe_2(CO)_9CpNiCo(CO)_3(C_2Ph_2)$ (**4a**) reaction as a model. At a

Table VIII. Atom Coordinates ($\times 10^4$) for $CpNiCoOs(CO)_6(C_2Ph_2)$ (**3a**)

	x	*y*	*z*
Ni	1209.3 (9)	2177.7 (11)	917.1 (4)
Co	3032.2 (9)	538.3 (11)	965.8 (4)
Os	3510.3 (3)	2956.7 (3)	544.3 (2)
C(1)	3379 (7)	710 (9)	235 (3)
O(1)	3346 (6)	163 (6)	−176 (2)
C(2)	5392 (9)	3119 (9)	388 (3)
O(2)	6494 (6)	3225 (7)	295 (3)
C(3)	3276 (9)	4382 (10)	802 (3)
O(3)	3104 (8)	5937 (7)	967 (3)
C(4)	2932 (9)	3370 (9)	−190 (3)
O(4)	2624 (8)	3586 (8)	−617 (2)
C(5)	1711 (8)	−712 (9)	937 (3)
O(5)	915 (7)	−1548 (7)	920 (3)
C(6)	4374 (9)	−624 (9)	1154 (3)
O(6)	5210 (7)	−1372 (8)	1265 (3)
C(7)	1805 (7)	1934 (8)	2071 (3)
C(8)	2204 (8)	2873 (8)	2472 (3)
C(9)	1641 (10)	2831 (10)	2987 (3)
C(10)	675 (9)	1849 (10)	3098 (3)
C(11)	246 (8)	926 (10)	2701 (3)
C(12)	806 (7)	954 (9)	2201 (3)
C(13)	2379 (7)	2007 (7)	1520 (3)
C(14)	3679 (7)	2314 (8)	1371 (3)
C(15)	4843 (7)	2473 (8)	1737 (3)
C(16)	5118 (8)	1518 (9)	2141 (3)
C(17)	6163 (9)	1727 (10)	2511 (4)
C(18)	6949 (9)	2890 (10)	2468 (4)
C(19)	6721 (8)	3854 (10)	2067 (3)
C(20)	5683 (8)	3636 (9)	1707 (3)
C(21)	−550 (9)	3179 (12)	1160 (4)
C(22)	−906 (8)	1830 (12)	1046 (4)
C(23)	−613 (9)	1620 (11)	489 (4)
C(24)	−89 (9)	2847 (13)	303 (4)
C(25)	−51 (10)	3801 (12)	713 (5)

Table IX. Bond Distances (Å) and Angles (deg) for $CpNiCoOs(CO)_6(C_2Ph_2)$ (**3a**)

Ni–Os	2.579 (1)	Co–C(14)	2.067 (8)
Ni–Co	2.394 (1)	Ni–Cp(ctr)	1.755 (1)
Co–Os	2.570 (1)	Ni–C(13)	1.900 (7)
Os–C(1)	2.273 (9)	C(7)–C(13)	1.485 (10)
Os–C(2)	1.919 (9)	C(13)–C(14)	1.377 (10)
Os–C(3)	1.908 (9)	C(14)–C(15)	1.477 (10)
Os–C(4)	1.949 (8)	C(1)–O(1)	1.148 (10)
Os–C(14)	2.147 (7)	C(2)–O(2)	1.126 (11)
Co–C(1)	1.853 (9)	C(3)–O(3)	1.141 (11)
Co–C(5)	1.774 (8)	C(4)–O(4)	1.122 (10)
Co–C(6)	1.794 (9)	C(5)–O(5)	1.122 (10)
Co–C(13)	2.065 (7)	C(6)–O(6)	1.128 (10)
Ni–Co–Os	62.49 (4)	Co–C(6)–O(6)	178.7 (8)
Ni–Os–Co	55.41 (3)	Os–C(1)–Co	76.3 (3)
Os–Ni–Co	62.10 (4)	Ni–C(13)–Co	74.2 (2)
Os–C(1)–O(1)	136.2 (8)	Ni–C(13)–C(14)	110.2 (5)
Os–C(2)–O(2)	179.4 (8)	Os–C(14)–Co	75.1 (2)
Os–C(3)–O(3)	177.8 (8)	Os–C(14)–C(13)	104.1 (5)
Os–C(4)–O(4)	178.3 (8)	Co–Os–C(1)	44.5 (2)
Co–C(1)–O(1)	147.3 (7)	Os–Co–C(1)	59.2 (3)
Co–C(5)–O(5)	177.1 (8)		

Table X. Spectroscopic Data for $CpNiCoM(CO)_6(C_2RR')$ (M = Fe, Ru, Os)

compd	color	ν(CO) (hexanes), cm^{-1}	ν(CO) (KBr), cm^{-1}	^1H NMR ($CDCl_3$), δ	m/z^a (rel intens)
$CpNiCoFe(CO)_6(C_2Ph_2)$ (**1a**)	light brown	2069 s, 2024 s, 2020 s, 2006 m, 1970 m, 1965 m	2067 s, 2016 s, br, 1971 s	5.05 s (Cp), 7.1–7.3 m (Ph)	584 (10), 556 (30), 528 (25), 500 (46), 472 (85), 444 (100), 416 (65)
$CpNiCoRu(CO)_6(C_2Ph_2)$ (**2a**)	dark brown	2072 s, 2043 vs, 2010 s, 2002 s, 1885 w, br	2072 s, 2051 s, 2046 s, 2015 s, 2008 s, 1985 s, 1865 s	5.13 s (Cp), 7.1–7.3 m (Ph)	630 (3), 602 (12), 574 (8), 546 (4), 518 (30), 490 (15), 462 (80)
$CpNiCoOs(CO)_6(C_2Ph_2)$ (**3a**)	dark brown	2072 s, 2041 s, 2015 m, 2002 s, 1989 s, 1973 m, 1884 w, br	2069 s, 2044 s, 2000 vs, 1983 s, 1858 s	5.07 s (Cp), 7.1–7.4 m (Ph)	720 (5), 692 (60), 664 (85), 636 (12), 608 (100), 580 (18), 552 (75)
$CpNiCoFe(CO)_6(C_2Et_2)$ (**1b**)	green	2065 s, 2021 vs, 2013 s, 2004 s, 1972 m, 1968 m	2064 s, 2013 s, br, 1959 m	1.41 t, 1.63 t (CH_3), 2.47 m, 2.60 m, 2.82 m, 3.04 m (CH_2), 5.20 s (Cp)	488 (5), 460 (20), 432 (20), 404 (15), 376 (18), 348 (100), 320 (42)
$CpNiCoRu(CO)_6(C_2Et_2)$ (**2b**)	dark brown	2068 s, 2035 vs, 2005 s, 1980 w, 1894 w, br	2065 s, 2027 s, 1997 s, br, 1874 m, br	1.24 t, 1.37 t (CH_3), 2.20 m, 2.50 m, 2.78 m (CH_2), 5.25 s (Cp)	534 (19), 506 (22), 478 (18), 450 (40), 422 (100), 394 (100), 366 (75)
$CpNiCoOs(CO)_6(C_2Et_2)$ (**3b**)	dark brown	2068 s, 2036 vs, 2008 s, 2002 s, 1981 m, 1970 m, 1874 vw, br	2065 s, 2031 s, 1998 s, 1967 m, sh, 1875 vw, br	1.33 t, 1.47 t, (CH_3), 2.62 m, 2.72 m, 2.87 m (CH_2), 5.32 s (Cp)	624 (14), 596 (22), 568 (26), 540 (52), 512 (46), 484 (100), 456 (65)
$CpNiCoFe(CO)_6(MeC_2Ph)$ (**1c**)	green	2067 s, 2021 vs, 2006 s, 1980 m, 1972 m, 1967 m	2053 s, 2050 s, 2029 m, sh, 1996 s, br	2.62 s, 2.68 s (Me), 4.94 s, 5.22 s (Cp), 7.1–7.3 m (Ph)	522 (3), 494 (19), 466 (20), 438 (18), 410 (29), 382 (93), 354 (100)
$CpNiCoRu(CO)_6(MeC_2Ph)$ (**2c**)	brown	2071 s, 2039 vs, 2008 s, 1998 s, 1887 w	2069 s, 2033 s, 1996 s, br, 1876 m	2.31 s, 2.64 s (Me), 4.90 s, 5.22 s (Cp), 7.1–7.4 m (Ph)	568 (3), 540 (10), 512 (9), 484 (9), 456 (30), 428 (29), 400 (100)
$CpNiCoOs(CO)_6(MeC_2Ph)$ (**3c**)	dark brown	2069 s, 2040 vs, 2011 m, 2002 s, 1985 m, 1972 m, 1886 w, br	2066 s, 2033 s, 1993 s, br, 1871 m, br	2.53 s, 2.79 s (Me), 4.97 s, 5.27 s (Cp), 7.1–7.4 m (Ph)	658 (2), 630 (20), 602 (20), 574 (14), 546 (100), 518 (16), 488 (85)
$CpNiCoFe(CO)_5(PPh_3)(C_2Ph_2)$ (**1d**)	dark brown	2039 s, 1974 s, 1969 s	2040 s, 1965 s, br, 1827 m	4.72 s (Cp), 7.1–7.4 m (Ph)	846 (0.5), 818 (5), 790 (7), 762 (4), 734 (10), 706 (11), 444 (30), 262 (100)

[a] For ^{56}Fe, ^{58}Ni, ^{102}Ru, and ^{192}Os.

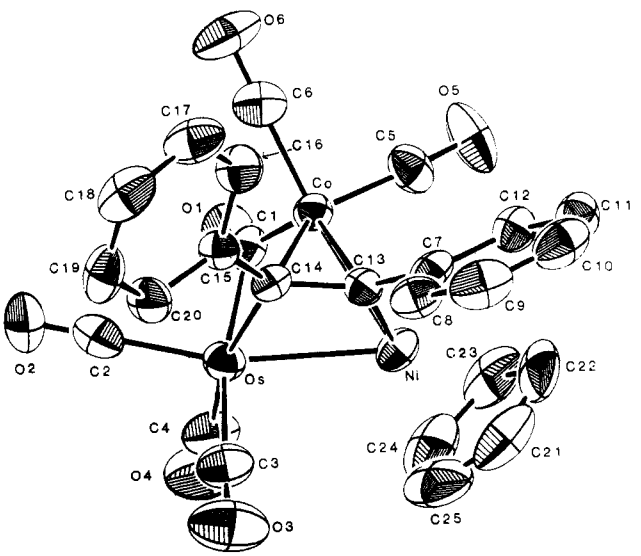

Figure 5. Structure of $CpNiCoOs(CO)_6(C_2Ph_2)$ (**3a**).

reaction temperature of 40–45 °C overnight the proportion of $Fe_3(CO)_{12}$ produced was increased and several side products were observed to be present by IR spectroscopy. Two that were isolated in reasonable yields and identified by IR and mass spectra were $Cp_2Fe_2(CO)_4$ and black $Fe_3(CO)_9(C_2Ph_2)$.[12] Reactions conducted in Et_2O or THF resulted in poor yields of the desired product, but again $Fe_3(CO)_{12}$ and $Fe_3(CO)_9(C_2Ph_2)$ were favored, with yields of the latter frequently about 30%. Replacing $Fe_2(CO)_9$ by $Fe(CO)_5$ increased the proportion of side products, especially $Cp_2Ni_2Fe_2(CO)_6(C_2Ph_2)$,[13] and decreased **1a**. Employing $Fe_3(CO)_{12}$ instead was even less effective, irrespective of the solvent. In refluxing hexane for 18 h, reaction of $Fe_3(CO)_{12}$ and **4a** yielded, after chromatography on Florisil, $Co_2(CO)_6(C_2Ph_2)$ (**5a**) and $Fe(CO)_5$ (eluted with hexane). Hexane/CH_2Cl_2 (4:1) then eluted small and variable amounts of **1a** (brown band), $Cp_2Ni_2Fe_2(CO)_6(C_2Ph_2)$ (blue band; ν(CO) 2010 s, 1973 s cm^{-1}), $Cp_2Ni_2Fe(CO)_3(C_2Ph_2)$ (green-brown band; ν(CO) 2030 vs, 1979 s, 1963 m cm^{-1}), and $Fe_3(CO)_9(C_2Ph_2)$ (brown-black band), and then CH_2Cl_2 eluted $Cp_2Fe_2(CO)_4$.

The formation of $CpNiCoRu(CO)_6(C_2Ph_2)$ (**2a**), $CpNiCoRu(CO)_6(C_2Et_2)$ (**2b**), and $CpNiCoRu(CO)_6(MeC_2Ph)$ (**2c**) was effective when $Ru(CO)_5$ was reacted with **4a–c**. The yields were low (10–15%), but the $Ru(CO)_5$ that did not react could be recovered by chromatography as $Ru_3(CO)_{12}$, reconverted to $Ru(CO)_5$, and reused. The use of $Ru_3(CO)_{12}$ itself was ineffective and produced (in hexane at 60 °C for 16 h) only trace amounts of the desired clusters **2a–c**.

The synthesis of the osmium analogues, $CpNiCoOs(CO)_6(C_2Ph_2)$ (**3a**), $CpNiCoOs(CO)_6(C_2Et_2)$ (**3b**), and $CpNiCoOs(CO)_6(MeC_2Ph)$ (**3c**), was similar to that of the ruthenium clusters. Again, only $Os(CO)_5$ (but not $Os_3(CO)_{12}$) was successful as a starting material. At higher temperatures (60 °C, 16 h), $Os_3(CO)_{12}$ did yield a trace of the desired product but offered

(12) Blount, J. F.; Dahl, L. F.; Hoogzand, C.; Hübel, W. *J. Am. Chem. Soc.* **1966**, *88*, 292.

(13) Sappa, E.; Tiripicchio, A.; Tiripicchio-Camellini, M. *J. Organomet. Chem.* **1980**, *199*, 243.

no advantage to the use of $Os(CO)_5$ at lower temperatures.

The heterotrimetallic alkyne clusters are green or brown solids, soluble in hydrocarbon solvents, and are not particularly air-sensitive. Their spectroscopic properties are given in Table X. The mass spectra exhibit relatively weak parent ion peaks and higher intensity ones for the successive loss of six CO groups. The phosphine complex **1d** shows the loss of five CO groups followed by PPh_3 and a prominent peak for PPh_3 itself (m/e 262).

Solid-State Structures. The structures have been determined for $CpNiCoFe(CO)_6(C_2Et_2)$ (**1b**), $CpNiCoRu(CO)_6(C_2Ph_2)$ (**2a**), and $CpNiCoOs(CO)_6(C_2Ph_2)$ (**3a**) in order that the effect of the replacement of iron by its congeners on the structures might be studied. Ideally, a structure of the iron–C_2Ph_2 complex **1a** would have been preferred, but it could not be suitably crystallized. Nevertheless, we believe that no crucial differences are incurred by the variation in alkyne substituent. A PPh_3 derivative of **1a**, $CpNiCoFe(CO)_5(PPh_3)(C_2Ph_2)$ (**1d**), could be crystallized, and its structure was determined. But, as shall be seen, the introduction of the PPh_3 group causes structural changes to occur that make the PPh_3 complex most certainly not representative of the parent iron hexacarbonyl cluster, but interestingly, it shares characteristics with the structures of the ruthenium and osmium hexacarbonyl clusters. The details of the individual crystal structures are discussed below. Here, we wish only to present the important features that, taken with the solid-state IR spectra, provide an overview of the different structural properties of members of this series.

The iron complex $CpNiCoFe(CO)_6(C_2Et_2)$ (**1b**) has a structure in which all CO groups are terminal, and the alkyne group is located parallel to the Ni–Co edge.

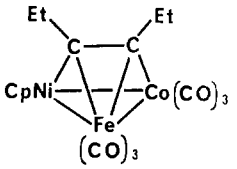

1b

There is every reason to believe that the structures of the C_2Ph_2 and MeC_2Ph compounds **1a** and **1d** are similar as all three exhibit closely similar ν(CO) spectra (Table X), with only absorptions for terminal CO groups.[14] In KBr there are essentially three strong bands, near 2067, 2016, and 1971 cm^{-1} (**1a**). The increased resolution in hexane solution reveals the six ν(CO) bands, all terminal, at 2069, 2024, 2020, 2006, 1970, and 1965 cm^{-1} (**1a**), expected for the asymmetric molecule, suggesting that the structure is preserved in hexane, and no IR-detectable amount of any other isomer is present.

The ruthenium and osmium complexes $CpNiCoRu(CO)_6(C_2Ph_2)$ (**2a**) and $CpNiCoOs(CO)_6(C_2Ph_2)$ (**3a**) have structures in which the orientation of the alkyne group has changed dramatically compared with that of iron complex **1b**. It is now

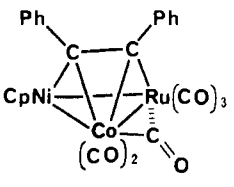

2a

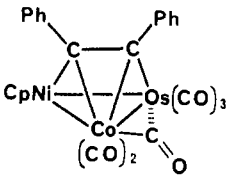

3a

oriented parallel to the Ni–Ru or Ni–Os edge. In addition, one of the "cobalt" CO groups now adopts a semibridging position across the Co–Ru or Co–Os bond.

The solid-state IR spectra (KBr) demonstrate the presence of the bridging carbonyl group in **2a** and **3a** by a strong absorption band at 1865 and 1858 cm^{-1}, respectively. In hexane solution, the bridging ν(CO) absorption is relatively weaker and occurs near 1885 cm^{-1}, but the presence of four to six ν(CO) terminal absorptions again suggests that the structure is probably maintained in this solvent. Little change occurs in the general appearance of the spectra when the alkynes C_2Et_2 or MeC_2Ph are present, so we suspect that all the complexes **2a–c** and **3a–c** have similar structures in the solid state and in hexane solution.

Replacement of a carbonyl group on cobalt by PPh_3 to form the iron complex **1d** brings about a remarkable structural change to produce a configuration that also possesses the two features that we have just associated with the ruthenium and osmium hexacarbonyl clusters. The alkyne is now oriented parallel to

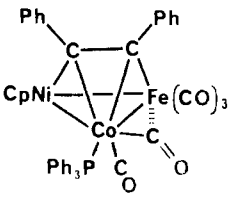

1d

the Ni–Fe bond, and one of the two remaining cobalt carbonyl groups adopts a semibridging position across the Co–Fe bond.

Once again, the presence of this carbonyl is observed in the solid-state IR spectrum (KBr) by absorption at 1827 cm^{-1}. In hexane, however, no such bridging ν(CO) band could be seen, so we cannot be sure that the structure of **1d** is maintained in this solvent.

How are these structural differences to be rationalized? In seeking an answer, it is worthwhile to compare these structures with those of other *nido*-M_3C_2 trimetallic alkyne clusters for which, as mentioned earlier, there are now some 20 determinations available for comparison. The orientation of the alkyne in them has recently been reviewed and the conclusion reached, supported by model calculations, that the orientation may be correlated with electron-accepting properties of the three metal fragments constituting the cluster.[4] In the preferred isomer, the more electron-attracting fragments appear to locate in the "basal" positions 2 or 3 rather than in the apical position 1 (**6**). Calculations

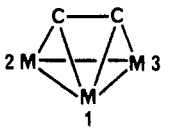

6

indicate that the alkyne behaves as an overall donor of electron density and bonds most strongly to positions 2 and 3 so that the more electron-accepting fragments will locate at these positions.

Thus, if the various clusters with CpNi, $Co(CO)_3$, and $Fe(CO)_3$ fragments are examined, we see a rationale for the least electron-attracting $Fe(CO)_3$ group always locating in apical position 1 in $FeCo_2(CO)_9C_2Et_2$,[15] $[CpNiFe_2(CO)_6(C_2Ph_2)]^-$,[16] $CpNiFeCo(CO)_6(PhC_2CO_2\text{-}i\text{-}Pr)$,[6] $Cp_2Ni_2Fe(CO)_3(C_2Ph_2)$,[17] and $Cp_2Ni_2Fe(CO)_3(PhC_2CO_2\text{-}i\text{-}Pr)$.[6] The structures of $CpNiFeCo(CO)_6(C_2RR')$ complexes **1a–c** in this study are then seen to conform to this pattern also, with the CpNi and $Co(CO)_3$ groups basal and the $Fe(CO)_3$ group apical. If this is the case, then perhaps the altered structure of phosphine derivative **1d**, where now the $Fe(CO)_3$ group is basal and the $Co(CO)_2(PPh_3)$ group is apical, results from a lowering of the electron-accepting nature of the cobalt fragment by PPh_3 substitution, to make this group less so than is $Fe(CO)_3$. This is a reasonable conjecture, but no calculations are presently available to support it.

The $Ru(CO)_3$ and $Os(CO)_3$ groups may be more electron-accepting than $Fe(CO)_3$, if the differing Pauling electronegativities of Fe (1.8), Ru (2.2), and Os (2.2) are a guide. (Note, however,

(14) This structure was also observed in the case of $CpNiCoFe(CO)_6(PhC_2CO_2\text{-}i\text{-}Pr)$.[6]

(15) Aime, S.; Milone, L.; Osella, D.; Tiripicchio, A.; Lanfredi, A. M. *Inorg. Chem.* **1982**, *21*, 501.
(16) Bruce, M. I.; Rodgers, J. R.; Snow, M. R.; Wong, F. S. *J. Organomet. Chem.* **1982**, *240*, 299.
(17) Sappa, E.; Lanfredi, A. M. M.; Tiripicchio, A. *J. Organomet. Chem.* **1981**, *221*, 93.

that Allred–Rochow electronegativity values (Fe, 1.64; Ru, 1.42; Os, 1.52) exhibit a different trend.) It is possible, then, that these heavier elements have a lowered preference for the apical position and, if they are more electron-accepting than $Co(CO)_3$, may locate in basal positions, as turns out to be the case. Again, calculations are lacking on this point, but there seems to be an established precedent since $Ru(CO)_3$ locates basally in $Co_2Ru(CO)_9(C_2Ph_2)$ in preference to a $Co(CO)_3$ group,[18] contrary to the structure of $Co_2Fe(CO)_9(C_2Et_2)$.[15]

Nonrigidity. The presence of the three different metals in these clusters provides for inherent chirality in the molecules, whether the alkyne substituents are identical or not. The ^1H NMR spectra (Table X) provide a useful probe for potential nonrigidity.

Compounds **1c**, **2c**, and **3c**, having the unsymmetrical alkyne PhC_2Me, are present in solution in both expected rotameric forms (e.g., **1c** and **1c'**), since the spectra at 400 MHz at room temperature show two Cp and two Me resonances and two phenyl

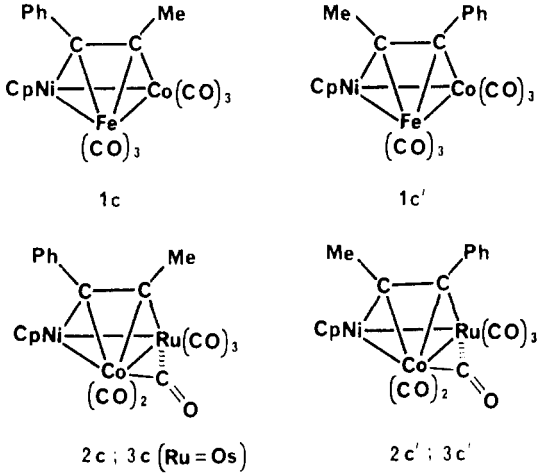

multiplets. Judging from the relative intensities, in each case the Cp and Me resonances having the lower chemical shift belong to one of the two rotamers. We tentatively assign these resonances to the rotamers illustrated as **1c–3c**, i.e. the ones that have the CPh group (and not the CMe) adjacent to NiCp. This is because a comparison of the NiCp resonance positions can be made with those of compounds **1a–3a**, which also have a CPh group adjacent to Ni, and with those of compounds **1b–3b**, which only have the aliphatic CEt group adjacent to Ni. The Cp chemical shift in the former set is consistently at lower δ values than in the latter. Hence, in the PhC_2Me compounds we consider that the lower Cp chemical shift probably reflects the presence of an adjacent phenyl group in this isomer (**1c–3c**), and correspondingly, the higher Cp resonance is from the other rotamer (**1c'–3c'**). An attempt to confirm this by an NOE experiment was unsuccessful, as no observable enhancement of either the Me or phenyl protons occurred on irradiating the Cp resonances. The relative proportions of the two rotamers of each complex at room temperature are quite solvent-dependent. Assuming the validity of our assignment, the ratios of isomer c': isomer c are approximately 1.25 ($CDCl_3$), 2.20 (Me_2CO), and 1.5 (toluene) for **1c**, 0.20, 0.42, and 0.30 for **2c**, and 0.40, 0.80, and 0.70 for **3c**.

Coalescence of the Cp or Me resonances was observed for all three clusters at higher temperatures[19] and results from a process that interconverts the c and c' rotamers. This may be viewed as the effective rotation of the alkyne C–C vector with respect to the face of the M_3 cluster. The ^1H NMR for the C_2Ph_2 complexes **1a**, **2a**, and **3a** exhibit the expected single Cp resonance and a complicated multiplet for the two magnetically inequivalent phenyls.

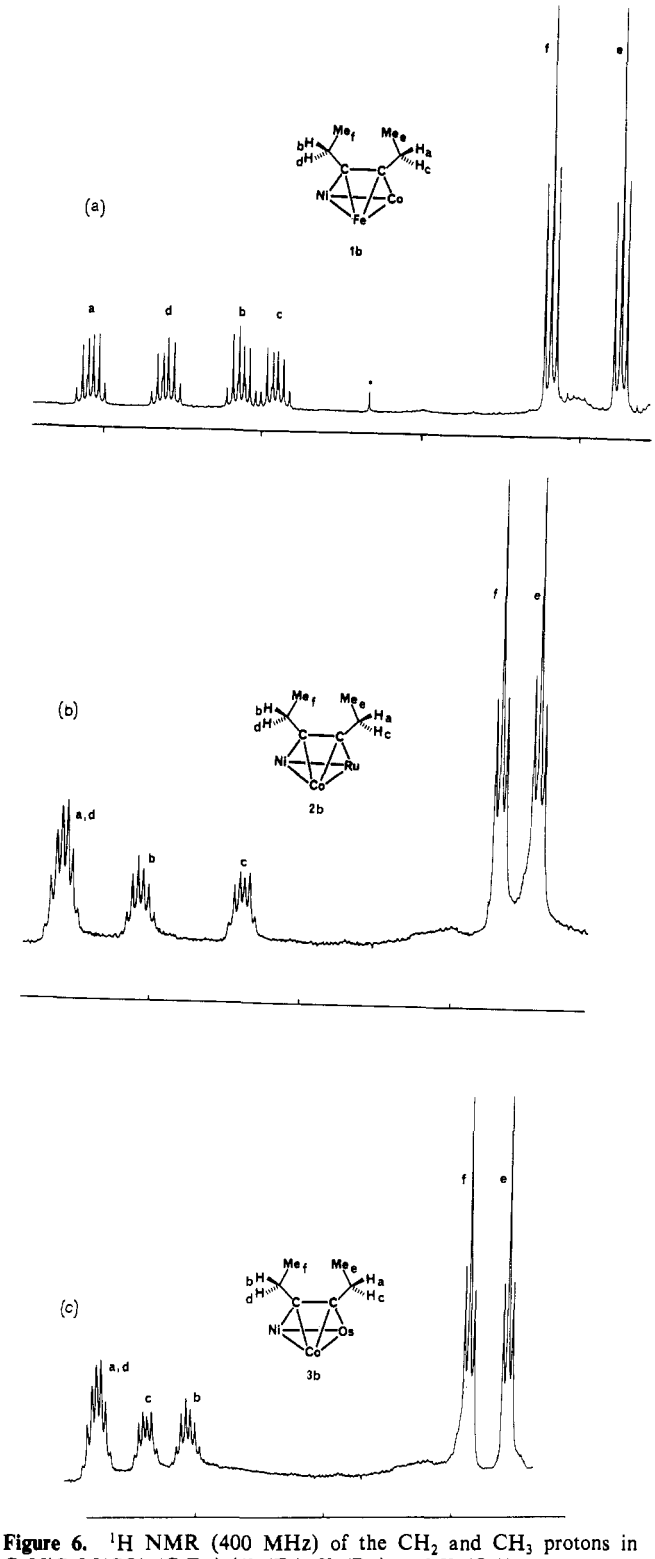

Figure 6. ^1H NMR (400 MHz) of the CH_2 and CH_3 protons in $CpNiCoM(CO)_6(C_2Et_2)$ (**1b** (Fe), **2b** (Ru), and **3b** (Os)) at room temperature. Proton assignments follow the text.

The fluxionality of these chiral clusters is revealed in more detail in the C_2Et_2 complexes **1b**, **2b**, and **2c** through the presence of the diastereotopic methylenes. Each ^1H NMR spectrum exhibits a single Cp resonance and two apparent methyl triplets but four multiplets in the methylene region, arising from the four magnetically nonequivalent hydrogens of the two diastereotopic CH_2 groups (Figure 6). In **1b**, these multiplets are well separated from one another and each consists essentially of two overlapping pairs of 1:3:3:1 quartets derived from coupling to the CH_3 group and to the geminal proton. In **2b** and **3b**, the two multiplets with greatest chemical shift are nearly superimposed. The assignment

(18) Braunstein, P.; Rose, J.; Bars, O. *J. Organomet. Chem.* **1983**, *252*, C101.
(19) Coalescence temperatures (K) and $\Delta G^{\ddagger}$ (kcal mol^{-1}) values obtained (toluene-d_8): **1c**, 339 (Me), 17.8; **2c**, 321 (Me), 330 (Cp), 16.8; **3c**, 315 (Me), 327 (Cp), 16.8. Estimates from the relative proportions at various temperatures (in toluene-d_8) are ground-state energy differences ΔE for the two rotamers (kcal mol^{-1}): **1c**, 0.19; **2c**, 0.70; **3c**, 0.24.

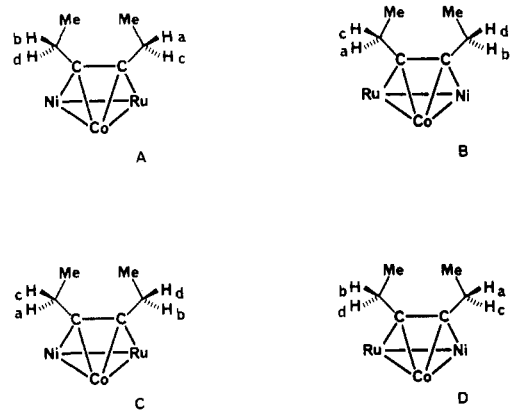

Figure 7. Scheme showing possible processes for the interconversion of methylene protons a–d in compound **2b**.

as to which CH_2 and CH_3 resonances are associated with the same Et group has been made by selective decoupling. This shows that resonances a, c, and e for **1b** are associated with one ethyl group and b, d, and f with the other. However, an NOE experiment for **1b** at either ambient temperature (294 K) or 202 K (at which exchange essentially is stopped) failed to exhibit any enhancement upon irradiation of the Cp resonance, so we are unable to go further in determining specifically which of the two different Et groups is responsible for a particular set of resonances, and they are arbitrarily assigned as shown in Figure 6.

The selective decoupling experiments done on the ruthenium or osmium cluster **2b** or **3b** at room temperature showed that exchange of the ethyl positions was also occurring, whereas none was seen for the iron compound **1b** at this temperature in the same experiment. Thus, in **2b**, irradiation of CH(b) caused not only decoupling of the methyl triplet (f) but disappearance of the CH(c) multiplet as a result of saturation transfer between b and c. Similarily, irradiation of CH(c) decouples the methyl triplet (e), and CH(b) disappears. This establishes that protons b and c on different methylenes are being interconverted by the exchange mechanism, as are a and d, and allows quite a clear picture of the exchange mechanism to be drawn.

With reference to Figure 7, it can be seen that four possible permutations, A–D, of the diastereotopic hydrogens can be visualized. A and B are related by a transformation that can be seen to equate to a transfer of the C_2Et_2 in A from the front face to the back face *without* any rotation of the acetylene C–C vector with respect to the Ni–Ru vector. C and D are similarly related to each other. A and C are related by a rotation of the acetylene with respect to the Ni–Ru vector, keeping it on the same face. A and D are related to each other by a combination of rotation and front-to-back face transfer.

Experimentally, we observe saturation transfer between CH protons on *different* methylene carbons but none between CH protons on the same carbon atom. This conclusively eliminates the conversion A ↔ B, since this process equilibrates hydrogens on the same carbon atoms only. We think it also eliminates the conversion A ↔ D, because it is difficult to conceive of a route for this conversion that does not essentially equate to either of the two-step processes A ↔ B ↔ D or A ↔ C ↔ D and in each case this involves a front-to-back face-transfer step A ↔ B that would exchange the hydrogens on the same carbon atom. This leaves process A ↔ C, which accounts for the observed saturation transfer as the exchange of the protons on different methylene carbons that are related in pairwise fashion by a local twofold axis (i.e., a ↔ d and b ↔ c). This gives the assignments displayed in Figure 6 and limits the fluxional process only to rotation of the alkyne on the face of the metal triangle without front-to-back face transfer occurring. The activation energy for this process for **1b**, determined by an inversion recovery experiment at temperatures above ambient, gave a value of $\Delta G^{\ddagger} = 17.8$ kcal mol^{-1}.

^{1}H NMR exchange in M_3C_2 alkyne clusters has been observed in other cases, and various mechanisms have been suggested. In a study of $H_2Ru_3(CO)_9$(cyclooctyne) and the osmium analogue, Deeming[20] obtained activation energies of 14.3 and 16.9 kcal mol^{-1}, respectively, and suggested that exchange resulted from a pivotal rearrangement, **7** → **9**, of the alkyne with respect to the triangular

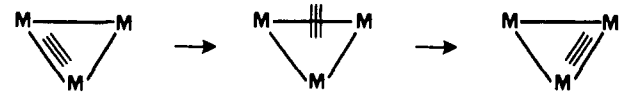

7 **8** **9**

metal face through the intermediacy of the closo configuration **8**.

If this process is envisaged to progress around all three vertices of the triangle, it produces, in asymmetric cluster **10**, the observed exchange of the alkyne substituents to give **11** and has the same result as a rotation of the alkyne ligand in place, including exchange of diastereotopic methylene protons in **1b–3b**.

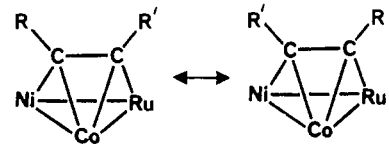

10 **11**

An alternative approach relates the fluxionality of *nido*-M_3C_2 clusters to their description as nido octahedra possessing one vacant site.[6] This view holds that the fluxionality is effectively the result of a migration of the vacant site over the "octahedral" cluster surface.

As can be seen in sequence **12–15**, a migration of the vacant site around one face of the octahedron by successive interchanges with a neighboring vertex in the same sense equally results in the observed exchange of the alkyne substituents R and R′.

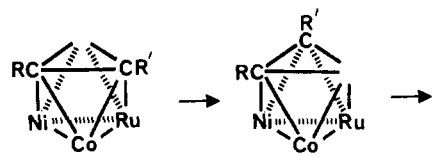

12 **13**

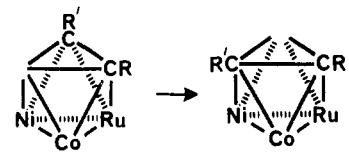

14 **15**

X-ray Crystal Structures. The structures have been determined for $CpNiCoFe(CO)_6(C_2Et_2)$ (**1b**), $CpNiCoFe(CO)_5(PPh_3)(C_2Ph_2)$ (**1d**), $CpNiCoRu(CO)_6(C_2Ph_2)$ (**2a**), and $CpNiCoOs(CO)_6(C_2Ph_2)$ (**3a**) and are illustrated in Figures 2–5, respectively. All consist of discrete molecules with no unusually short inter- or intramolecular contacts. In each case, the alkyne ligand is bonded to the trimetallic cluster in the μ_3-(η^2-$\|$)^5 or $(2\sigma + \pi)^1$ fashion to give a *nido*-M_3C_2 cluster overall. Iron compound **1a** has the alkyne C–C vector essentially parallel to the Ni–Co vector. In simple valence terminology, the alkyne is σ-bonded to Ni and Co and π-bonded to Fe (**16**). All CO groups are terminal, and each metal achieves an 18-electron count. The ruthenium and osmium compounds have the alkyne C–C vector instead parallel to the Ni–Ru or Ni–Os edge. A simple $(2\sigma + \pi)$ description, where the alkyne σ-bonds to these metals and π-bonds to Co, results in electron counts of 17 (Ru, Os), 18 (Ni), and 19 (Co), and it is notable that, in each case, one of the CO groups on cobalt adopts a semibridging[21] role in these two structures. Alternatively, a

(20) Deeming, A. J. *J. Organomet. Chem.* **1978**, *150*, 123.

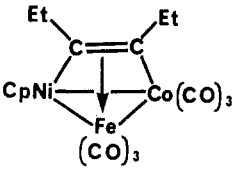

16

structure with a Co–Ru (Os) dative bond or equivalent semiionic description (**17**) may be drawn to satisfy the electron counts.

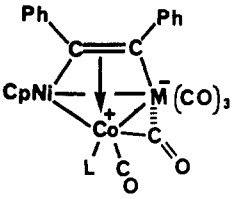

17 (L = CO; M = Ru, Os)
18 (L = PPh_3; M = Fe)

The alkyne group in the phosphine-substituted iron complex, **1d**, also displays this orientation and is likewise accompanied by a semibridging CO group (**18**).

These observations add further examples to a growing list that correlates the presence of a semibridging CO group with M_3C_2 alkyne structures that do not straightforwardly adhere to the 18-electron rule. It is found in $Cp_2NiFeMo(CO)_5(PhC_2CO_2$-*i*-$Pr)$,[6] $Co_2Ru(CO)_9(C_2Ph_2)$,[18] $Os_3(CO)_{10}(C_2Ph_2)$,[22] $Cp_2NiRu_2(CO)_4(C_2Ph_2)$,[23] and $Cp_2W_2Os(CO)_7[C_2(C_6H_4Me)_2]$.[24]

The different orientations of the alkyne group in NiFeCo compounds **1b** and **1d** are reflected in substantial differences in the metal–metal bond lengths in these two triangular metallocycles. The Ni–Co bond in **1b** is bridged by the alkyne as in **19**, and this

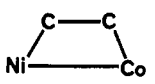

19

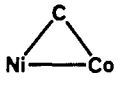

20

bond (2.432 (1) Å) is substantially longer than the corresponding bond in **1d**, **2a**, or **3a** (2.390 (4), 2.399 (1), and 2.394 (1) Å, respectively), where the alkyne bridges as in **20**. The Ni–Fe distances in **1b** (2.402 (1) Å) and **1d** (2.486 (4) Å), where a similar relationship applies, are also significantly different. But, in both **1b** and **1d**, the Co–Fe bond is bridged in a manner similar to that in **20**, and these bond lengths show the least differences being 2.494 (1) Å in **1b** and 2.469 (4) Å in **1d**. A nice example of how the disposition of the alkyne group can affect the metallocycle bond lengths is the case of $Cp_2W_2Os(CO)_7[C_2(C_6H_4Me)_2]$. The structures of two isomers of this cluster are available,[24] one with the alkyne vector parallel to the W–W bond and the other with it parallel to W–Os, and observed differences in W–W and W–Os bond lengths (ca. 0.12–0.14 Å) in arrangements comparable to those of **19** and **20** are considerably larger.

The Ni–Cp moiety is present in all four structures, and its dimensions show little variation. The Ni–Cp(centroid) distances are all near 1.75 Å. The Cp group is in all cases displaced from having its plane normal to that of the NiCoM metallocycle in a direction away from the face bearing the alkyne, and the displacements are comparable, as illustrated by the dihedral angles between these planes of 68.8 (4), 71.8 (5), 69.6 (3), and 70.3 (3)° for **1b**, **1d**, **2a**, and **3a**, respectively.

The interaction of the alkyne ligand with the metallic cluster leads to a lengthening of the alkyne C–C bond to a distance of 1.34 (2)–1.377 (10) Å in these compounds, which is in the olefinic range typically observed.[1] The dihedral angles between the NiCoM plane and the metal–alkyne skeletal plane **19** (or its equivalent) are all near 57° and range from 57.1 (1)° in **1b** to 57.8 (3)° in **1d**. These are similar to other reported values, for example those for $Cp_3Ru_3(CO)(C_2Ph_2)$ (57.5 (2)°) and $Cp_3Rh_3(CO)[C_2(C_6F_5)_2]$ (56.0 (2)°).[25] The plane of the four skeletal carbon atoms of the alkyne itself is tipped out of this plane just mentioned, in a direction away from the NiCoM plane, as indicated by the dihedral angle between it and the last one. This ranges from 70.5, 71.5, and 72.2° in **2a**, **3a**, and **1b**, respectively, to 77.0° in the phosphine, **1d**. The additional tilt in the last complex is in a direction away from the phosphine-bearing cobalt. The magnitudes of the angles are in general agreement with those observed previously.[4]

The semibridging CO group (**21**) that is present in **2a**, **3a**, and **1d** has a similar geometry in each case and compares well with the dimensions found in the several other examples that occur in related alkyne clusters.[6,18,22-24] The lower precision of **1d** makes a full comparison that includes this structure difficult.

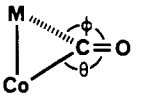

21

The Co–C bond lengths are 1.158 (9) Å (**2a**), 1.148 (10) Å (**3a**), and 1.19 (3) Å (**1d**), and the corresponding M---C bond lengths are 2.251 (8) Å (**2a**), 2.273 (8) Å (**3a**), and 2.07 (1) Å (**1d**). The Co–CO group is considerably distorted from linearity, as indicated by θ angles of 148.2 (7)° (**2a**), 147.3 (7)° (**3a**), and 148 (1)° (**1d**) and ϕ angles of 134.5 (6)° (**2a**), 136.2 (7)° (**3a**), and 131 (1)° (**1d**).

Acknowledgment. This work was supported by the Natural Sciences and Engineering Research Council of Canada, through operating grants to F.W.B.E., D.S., and A.S.T.

Registry No. **1a**, 101316-16-9; **1b**, 101316-15-8; **1c**, 101316-17-0; **1c'**, 101316-18-1; **1d**, 101316-09-0; **2a**, 101316-07-8; **2b**, 101316-10-3; **2c**, 101316-11-4; **2c'**, 101316-14-7; **3a**, 101316-08-9; **3b**, 101349-49-9; **3c**, 101316-12-5; **3c'**, 101316-13-6; **4a**, 66752-82-7; **4b**, 101316-19-2; **4c**, 72347-02-5; $Fe_2(CO)_9$, 15321-51-4; $Ru(CO)_5$, 16406-48-7; $Os(CO)_5$, 16406-49-8; Ni, 7440-02-0; Co, 7440-48-4; Fe, 7439-89-6; Ru, 7440-18-8; Os, 7440-04-2.

Supplementary Material Available: Tables of anisotropic thermal parameters, calculated hydrogen atom coordinates, calculated mean planes and dihedral angles, and calculated and observed structure amplitudes for $CpNiCoFe(CO)_6(C_2Et_2)$ (**1b**) (Tables S1–S4), $CpNiCoFe(CO)_6(PPh_3)(C_2Ph_2)$ (**1d**) (Tables S5–S8), $CpNiCoRu(CO)_6(C_2Ph_2)$ (**2a**) (Tables S9–S12), and $CpNiCoOs(CO)_6(C_2Ph_2)$ (**3a**) (Tables S13–S16) (73 pages). Ordering information is given on any current masthead page.

(21) Cotton, F. A. *Prog. Inorg. Chem.* **1976**, *21*, 1.
(22) Pierpoint, C. G. *Inorg. Chem.* **1977**, *16*, 636.
(23) Sappa, E.; Tiripicchio, A.; Tiripicchio-Camellini, M. *J. Organomet. Chem.* **1981**, *213*, 175.
(24) (a) Churchill, M. R.; Bueno, C.; Wasserman, J. J. *Inorg. Chem.* **1982**, *21*, 640. (b) Busetto, L.; Green, M.; Hessner, B.; Howard, J. A. K.; Jeffrey, J. C.; Stone, F. G. A. *J. Chem. Soc., Dalton Trans.* **1983**, 519.
(25) Trinh-Toan; Broach, R. W.; Gardner, S. A.; Rausch, M. D.; Dahl, L. F. *Inorg. Chem.* **1977**, *16*, 279.